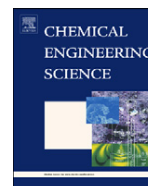




Contents lists available at SciVerse ScienceDirect

Chemical Engineering Science

journal homepage: www.elsevier.com/locate/ces

Buoyancy-driven pattern formation in reactive immiscible two-layer systems

D.A. Bratsun^a, A. De Wit^{b,*}^a Theoretical Physics Department, Perm State Pedagogical University, Ulitsa Sibirskaya 24, 614600 Perm, Russia^b Nonlinear Physical Chemistry Unit, Service de Chimie Physique et Biologie Théorique, Faculté des Sciences, CP 231, Université Libre de Bruxelles (U.L.B.), 1050 Brussels, Belgium

ARTICLE INFO

Article history:

Received 21 October 2010

Received in revised form

4 June 2011

Accepted 4 August 2011

Available online 23 August 2011

Keywords:

Chemo-hydrodynamics

Convection

Fingering

Interface

Rayleigh–Taylor

Buoyancy

ABSTRACT

Buoyancy-driven convection can be induced by concentration and temperature gradients near the interface between two immiscible fluids filling a vertical Hele–Shaw cell, each of them containing a reactant of an exothermic $A+B\rightarrow C$ reaction taking place in the bulk of the lower layer. A chemo-hydrodynamical pattern appears then due to the combined action of Rayleigh–Taylor, diffusive layer convection and Rayleigh–Bénard instabilities occurring either below or above the interface. The mathematical model we develop to describe such dynamics consists in a set of reaction–diffusion–advection equations ruling the evolution of concentrations and temperature coupled to Navier–Stokes equation, written in a Hele–Shaw approximation. We perform numerical simulations of the non-linear system and study the influence on pattern formation of changes in the Damköhler number of the problem and in the ratio of initial reactant concentrations.

© 2011 Elsevier Ltd. All rights reserved.

1. Introduction

Formation and dynamic evolution of patterns are at the core of numerous studies in both hydrodynamic and reaction–diffusion (RD) systems. In the last years, an increasing number of works has been devoted to the study of patterns that emerge when RD and hydrodynamic mechanisms are put at work together. In this framework, the study of buoyancy-driven fingering in a reactive two-layer system of immiscible fluids is interesting both from a fundamental point of view and with respect to potential applications ranging from petroleum engineering, extraction of plutonium salt to pharmaceutical engineering and food production. The spontaneous generation of convective flows in immiscible two-layer systems is of practical importance because convection leads to mechanisms of mass transfer from one fluid phase to the other much more intensive than molecular diffusion and can drastically alter pattern formation in the system. One of such mechanism results from a buoyancy-induced chemo-hydrodynamical instability of Rayleigh–Taylor type due to the existence of statically unstable density profiles in the gravity field. Such unfavorable density stratifications generate spontaneous convective flows near the liquid–liquid interface. This happens, for example, when either one of the reactants or the product solution in the bulk or close to the interface is denser than the surrounding liquid. Under the action of gravity the denser liquid sinks into the

less dense one inducing a convective pattern which progresses in time. Such chemically driven buoyancy-related patterns have received increasing attention during the last years both from experimental (Sherwood and Wei, 1957; Micheau et al., 1983; Avnir and Kagan, 1984, 1995; Pons et al., 2000; Ermakov et al., 2001; Karlov et al., 2002) and theoretical (Citri et al., 1990; Pérez-Villar et al., 2000; Bees et al., 2001) point of view. Recently, convective phenomena related to such buoyancy effects due to an exothermic $A+B\rightarrow C$ neutralization reaction close to an immiscible liquid–liquid interface have been studied experimentally by Eckert and Grahn (1999), Eckert et al. (2004), Bratsun et al. (2005), Shi et al. (2005), Shi and Eckert (2006, 2007). Depending on the nature of the reactants used, Marangoni effects due to surface tension gradients can come into play as well (Bratsun et al., 2005; Shi et al., 2005; Shi and Eckert, 2006, 2007; Grahn, 2006; Bratsun and De Wit, 2004). Their experimental system consists in an organic solution containing an acid (reactant A) put in contact in a Hele–Shaw cell with an aqueous solution in which a base (reactant B) is dissolved. After transfer of the acid across the interface, a neutralization reaction takes place in the aqueous phase. In the absence of Marangoni effects, dynamics and patterns in the form of plumes rising above the interface and fingers falling below it are observed (Eckert and Grahn, 1999; Eckert et al., 2004). They result from the coupling between different buoyancy-driven instabilities, such as Rayleigh–Taylor, diffusive-layer convection (DLC), Rayleigh–Bénard and double diffusive instabilities (Trevelyan et al., 2011).

Similar experiments have been conducted in parallel using miscible solvents. In this case a less dense aqueous solution of

* Corresponding author.

E-mail address: adewit@ulb.ac.be (A. De Wit).

a given acid is put in contact from the above with a miscible denser aqueous solution of a simple base (Zalts et al., 2008; Almarcha et al., 2010a,b). Buoyancy-driven patterns are observed which are quite different from those observed in the immiscible case: only ascending plumes are obtained above the initial contact line while a planar reaction front moves downwards (Almarcha et al., 2010a). In some cases, convective deformations are also observed after a longer time below the initial contact line (Zalts et al., 2008) but this has been shown to be due to the interference of the color indicator used for visualization purposes (Almarcha et al., 2010b). It is interesting to note that, in miscible systems, the patterns observed are asymmetric with regard to the contact line between both solvents, a peculiarity related to the reaction and thus not observed in non-reactive systems where buoyancy-driven instabilities have up–down symmetries (Trevelyan et al., 2011). This up–down symmetry with regard to the contact line is also broken when the two solvents are immiscible however reaction–diffusion–convection (RDC) patterns are quite different from those in the miscible reactive case even if similar reactants are used. As an example, the patterns studied by Eckert and Grahn (1999) using simple carboxylic acids in an organic phase above immiscible water containing sodium hydroxide (NaOH) are quite different from those observed in the same geometry when chlorhydric acid (HCl) is put on top of NaOH in miscible aqueous solutions (Almarcha et al., 2010a, 2011) especially below the contact line. Even if, in both cases, ascending plumes develop above the line of contact, no convection is obtained in the miscible case below it while descending plumes are obtained in the immiscible case.

In this framework, the present work aims to study numerically the chemo-hydrodynamic patterns which can result from buoyancy effects in vertical reactive immiscible two-layer systems. We analyze the coupling between a simple exothermic $A+B\rightarrow C$ reaction and gravity-driven convection in a setup similar to the one studied experimentally using immiscible solvents by Eckert and Grahn (1999) and Eckert et al. (2004). Our goal is, in particular, to describe the falling fingers observed below the interface as a function of the parameters of the problem. Our analysis is based on numerical integration of a two-dimensional (2D) model coupling Navier–Stokes equations for the evolution of the flow velocity in both layers coupled to RDC equations for the concentrations of the relevant chemical species and temperature. We study numerically the spatio-temporal dynamics that can be observed due to unfavorable density profiles appearing in the system when the reaction starts to take place upon diffusion of the reactant dissolved in the upper layer toward the lower layer. We analyze numerically the influence of the ratio between the characteristic hydrodynamic and chemical time scales (i.e. the role of the Damköhler number of the problem) and of the ratio of the initial concentrations of reactants on the spatio-temporal dynamics of concentration and flow velocity. We compare our numerical results with those obtained experimentally (Eckert and Grahn, 1999; Eckert et al., 2004) and discuss also the differences and analogies with the miscible case.

In this regard, the article is organized as follows: in Section 2 we formulate the problem and discuss all aspects of the proposed mathematical model. The details of the numerical method are given in Section 3 while Section 4 gives the numerical results and comparison with experimental data. Section 5 summarizes the results and provides some discussion.

2. Theoretical model

The system we consider consists in two vertical parallel solid plates separated by a thin gap containing two immiscible incompressible liquid solvents, separated by a plain and undeformable interface (see Fig. 1). A reactant A dissolved in the upper solvent can diffuse down through the interface to react with another

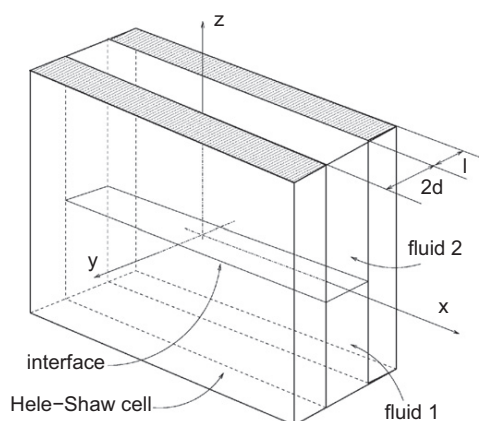


Fig. 1. Geometrical configuration of the two-layer system and coordinate axes.

reactant B dissolved in the lower layer. The reaction $A+B\rightarrow C$ forms a product C in an exothermic reaction with enthalpy Q . In our theoretical model, we assume that, as in experiments (Eckert and Grahn, 1999; Eckert et al., 2004), this exothermic reaction takes place solely in the lower phase as the reactant B is considered immiscible in the upper phase and that the product C does not dissolve in the upper layer (Eckert and Grahn, 1999). For simplicity, we also consider that the three chemical species A , B and C have the same diffusion coefficient in the lower phase. The concentrations of the chemical species are here small enough for the properties of the fluids to be independent of concentrations and Boussinesq approximation to be made. Concerning the flow, we assume that all phenomena related to surface tension are absent, i.e. Marangoni instabilities are negligible and the interface is undeformable.

We start with the standard set of RDC equations coupling Navier–Stokes Eq. (2) to evolution Eq. (3) for the temperature Θ and (4) and for the concentration Σ_j of species j :

$$\nabla \cdot \vec{U} = 0, \quad (1)$$

$$\frac{\partial \vec{U}}{\partial t} + \vec{U} \cdot \nabla \vec{U} = -\frac{1}{\rho_0} \nabla P + \nu \Delta \vec{U} + \frac{1}{\rho_0} \rho(\Theta, \Sigma_j) \vec{g}, \quad (2)$$

$$\frac{\partial \Theta}{\partial t} + \vec{U} \cdot \nabla \Theta = \chi \Delta \Theta - \frac{1}{C_p \rho_0} QR(\Theta, \Sigma_j), \quad (3)$$

$$\frac{\partial \Sigma_j}{\partial t} + \vec{U} \cdot \nabla \Sigma_j = D_j \Delta \Sigma_j + R(\Theta, \Sigma_j), \quad (4)$$

where Δ is the Laplacian in 3D, $\vec{U}(U_x, U_y, U_z)$ is the velocity, and P is the pressure. The density ρ_0 of the fluid, its kinematic viscosity ν , temperature diffusivity χ , heat capacity C_p and the diffusion coefficient D_j of the species j are constant. $R(\Theta, \Sigma_j)$ is the kinetic function of the problem while Q is the enthalpy of reaction. The boundary conditions at the solid plates are

$$y = \pm d: \quad \vec{U} = 0, \quad \frac{\partial \Theta}{\partial y} \pm \frac{1}{d} Bi(\Theta - \Theta_0) = 0, \quad \frac{\partial \Sigma_j}{\partial y} = 0. \quad (5)$$

The reference temperature Θ_0 is the room temperature at which the density of the fluid is $\rho = \rho_0$. The dimensionless Biot number, Bi , is defined as $Bi = d\gamma_T/\kappa$, where γ_T is the heat exchange coefficient between the fluid and the solid walls, $2d$ is the gap-width between the plates and κ is the thermal conductivity of the fluid. Depending on the composition of the Hele–Shaw plates and on their thickness l , the Biot number Bi may take a value from 0 (thermo-isolated plates) to ∞ (highly conductive plates).

We further assume that the gap-width $2d$ is small enough so that the fluid flow may be considered as quasi two-dimensional,

i.e. a Hele–Shaw approximation is applicable (Bratsun and De Wit, 2004). Taking into account the boundary conditions (5), the velocity, temperature and concentration profiles are assumed to be approximated by the following functions along the gap:

$$U_x(x,y,z) = \frac{3}{2} \left(1 - \frac{y^2}{d^2}\right) v_x(x,z),$$

$$U_y(x,y,z) = 0,$$

$$U_z(x,y,z) = \frac{3}{2} \left(1 - \frac{y^2}{d^2}\right) v_z(x,z),$$

$$\Theta(x,y,z) = \frac{3}{2} \frac{Bi}{(3+Bi)} \left(\frac{2}{Bi} + 1 - \frac{y^2}{d^2}\right) T(x,z),$$

$$\Sigma_j(x,y,z) = C_j(x,z), \quad (6)$$

where $\vec{v}(v_x, v_z)$ is the two-component velocity field while $T(x,z)$ and $C_j(x,z)$ are the 2D temperature and concentration fields obtained after averaging the 3D fields along the gap.

2D evolution equations in the Hele–Shaw approximation are obtained by inserting (6) into (1)–(4) and averaging with respect to the y -space direction perpendicular to the solid plates as

$$\langle \dots \rangle = \frac{1}{2d} \int_{-d}^d \dots dy.$$

This procedure reduces the system geometry to a 2D domain spanned by the x and z -coordinates and in which the evolution equations now read:

$$\nabla \cdot \vec{v} = 0,$$

$$\frac{\partial \vec{v}}{\partial t} + \frac{6}{5} \vec{v} \cdot \nabla \vec{v} = -\frac{1}{\rho_0} \nabla p + \nu \Delta \vec{v} - 3 \frac{\nu}{d^2} \vec{v} + \frac{1}{\rho_0} \langle \rho(\Theta, \Sigma) \rangle \vec{g},$$

$$\frac{\partial T}{\partial t} + \frac{3(5+2Bi)}{5(3+Bi)} \vec{v} \cdot \nabla T = \chi \Delta T - \frac{\chi}{d^2} \frac{3Bi}{(3+Bi)} T - \frac{1}{C_p \rho_0} \langle QR_j(\Theta, \Sigma) \rangle,$$

$$\frac{\partial C_j}{\partial t} + \vec{v} \cdot \nabla C_j = D_j \Delta C_j + \langle R_j(\Theta, \Sigma) \rangle, \quad (7)$$

where now $\Delta = \partial^2 / \partial x^2 + \partial^2 / \partial z^2$.

Taking into account that our system consists of two layers of immiscible fluids we divide the system geometry into two 2D sub regions $0 < x < H$, $-L_{bot} < z < L_{up}$ separated by a line $z=0$ standing for the interface. H is the width of the system while L_{bot} and L_{up} are the height of the lower and upper layers respectively. Let indexes $i=1,2$ correspond to the lower ($z < 0$) and upper ($z > 0$) layer respectively. To non-dimensionalize the problem, we choose the following characteristic scales: length $2d$, time $(2d)^2 / D_{A1}$, velocity $D_{A1} / 2d$, pressure $\rho_1 \nu_1 D_{A1} / (2d)^2$, concentrations A_0 and temperature $|Q| A_0 / \rho_1 C_{p1}$ where D_{A1} and A_0 are respectively the diffusion coefficient and the initial concentration of the reactant A in the upper layer while ρ_1, ν_1 and c_{p1} are the density, kinematic viscosity and heat capacity of the lower fluid. In addition, since, here, heat effects are not dominant, we assume that the solid walls are highly-conductive, i.e. $Bi \rightarrow \infty$. Considering a simple reaction scheme $A + B \rightarrow C$ with kinetic constant k_c , the dimensionless governing equations in the Boussinesq approximation can be written as follows: for the lower layer, we have

$$\nabla \cdot \vec{v}_1 = 0, \quad (8)$$

$$\frac{1}{Sc} \left(\frac{\partial \vec{v}_1}{\partial t} + \frac{6}{5} \vec{v}_1 \cdot \nabla \vec{v}_1 \right) = -\nabla p_1 + \Delta \vec{v}_1 - 12 \nu \vec{v}_1 + (LeRT_1 - R_A A_1 - R_B B - R_C C) \vec{z}, \quad (9)$$

$$\frac{\partial T_1}{\partial t} + \frac{6}{5} \vec{v}_1 \cdot \nabla T_1 = Le \Delta T_1 - 12 Le T_1 + D_a A_1 B, \quad (10)$$

$$\frac{\partial A_1}{\partial t} + \vec{v}_1 \cdot \nabla A_1 = \Delta A_1 - D_a A_1 B, \quad (11)$$

$$\frac{\partial B}{\partial t} + \vec{v}_1 \cdot \nabla B = \Delta B - D_a A_1 B, \quad (12)$$

$$\frac{\partial C}{\partial t} + \vec{v}_1 \cdot \nabla C = \Delta C + D_a A_1 B. \quad (13)$$

For the upper layer, we get

$$\nabla \cdot \vec{v}_2 = 0, \quad (14)$$

$$\frac{1}{Sc} \left(\frac{\partial \vec{v}_2}{\partial t} + \frac{6}{5} \vec{v}_2 \cdot \nabla \vec{v}_2 \right) = -\frac{1}{\rho} \nabla p_2 + \nu \Delta \vec{v}_2 - 12 \nu \vec{v}_2 + (\beta Le RT_2 - \beta_A R_A A_2) \vec{z}, \quad (15)$$

$$\frac{\partial T_2}{\partial t} + \frac{6}{5} \vec{v}_2 \cdot \nabla T_2 = \chi Le \Delta T_2 - 12 \chi Le T_2, \quad (16)$$

$$\frac{\partial A_2}{\partial t} + \vec{v}_2 \cdot \nabla A_2 = D \Delta A_2. \quad (17)$$

Here $T_i(x,z,t)$ the temperature field, $A_i(x,z,t)$, $B(x,z,t)$ and $C(x,z,t)$ are the concentrations of the reactants and product respectively. The full list of dimensionless parameters (Damköhler number D_a , Lewis number Le , thermal R and solutal R_A, R_B, R_C Rayleigh numbers, etc) which appear in Eqs. (8)–(17) is given in Table 1.

To simplify the problem and avoid adding additional parameters related to jump conditions for the variables at the interface, we assume continuity of these quantities at the interface, i.e. take the following boundary conditions:

$$z=0: \quad T_1 = T_2, \quad A_1 = A_2, \quad v_{z1} = v_{z2} = 0, \quad v_{x1} = v_{x2}, \quad (18)$$

$$\frac{\partial T_1}{\partial z} = \kappa \frac{\partial T_2}{\partial z}, \quad \frac{\partial A_1}{\partial z} = D \frac{\partial A_2}{\partial z}, \quad \frac{\partial v_{x1}}{\partial z} = \eta \frac{\partial v_{x2}}{\partial z}, \quad (19)$$

$$\frac{\partial B}{\partial z} = \frac{\partial C}{\partial z} = 0. \quad (20)$$

At the upper $z=L_{up}$ and lower $z=-L_{bot}$ horizontal boundaries, we assume no flow and no-flux boundary conditions for the concentrations and temperature. Periodic boundary conditions are applied at the vertical boundaries $x=0,H$. The initial conditions are

$$-L_{bot} < z < 0: \quad \vec{v}_1 = 0, \quad T_1 = 0, \quad A_1 = 0, \quad B = \frac{1}{\gamma}, \quad C = 0,$$

$$0 < z < L_{up}: \quad \vec{v}_2 = 0, \quad T_2 = 0, \quad A_2 = 1. \quad (21)$$

where $\gamma = A_0/B_0$ is the ratio between the initial concentrations of A and B initially present in the upper and lower layer respectively. This is typically the parameter which is varied in experiments.

Table 1
List of dimensionless parameters.

| | |
|---|--|
| $Sc = \nu_1 / D_{A1}$ | Schmidt number |
| $Le = \chi_1 / D_{A1}$ | Lewis number |
| $D_a = (2d)^2 k_c A_0 / D_{A1}$ | Damköhler number |
| $R = g \beta_T Q A_0 (2d)^3 / \kappa_1 \nu_1$ | Thermal Rayleigh number |
| $R_A = g \beta_{A1} A_0 (2d)^3 / D_{A1} \nu_1$ | Solutal Rayleigh number related to reactant A |
| $R_B = g \beta_B A_0 (2d)^3 / D_{A1} \nu_1$ | Solutal Rayleigh number related to reactant B |
| $R_C = g \beta_C A_0 (2d)^3 / D_{A1} \nu_1$ | Solutal Rayleigh number related to the product C |
| $\rho = \rho_2 / \rho_1$ | Density ratio |
| $\kappa = \kappa_2 / \kappa_1$ | Heat conductivity ratio |
| $\chi = \chi_2 / \chi_1$ | Heat diffusivity ratio |
| $\nu = \nu_2 / \nu_1$ | Kinematic viscosity ratio |
| $\eta = \eta_2 / \eta_1$ | Dynamic viscosity ratio |
| $\beta = \beta_{T2} / \beta_{T1}$ | Thermal expansion coefficient ratio |
| $\beta_A = \beta_{A2} / \beta_{A1}$ | Solutal expansion coefficient ratio |
| $D = D_{A2} / D_{A1}$ | Diffusivity ratio of A |
| $\gamma = A_0 / B_0$ | Initial concentration ratio |

Table 2
List of experimental data from Eckert et al. (2004).

| Lower layer | Upper layer | Ratio |
|--|---|------------------|
| $\eta_1 = 1.169 \times 10^{-3}$ Pa s | $\eta_2 = 1.122 \times 10^{-3}$ Pa s | $\eta = 0.96$ |
| $\nu_1 = 0.89 \times 10^{-6}$ m ² /s | $\nu_2 = 1.0 \times 10^{-6}$ m ² /s | $\nu = 1.1$ |
| $\kappa_1 = 0.566$ W/m K | $\kappa_2 = 0.131$ W/m K | $\kappa = 0.231$ |
| $\chi_1 = 1.43 \times 10^{-7}$ m ² /s | $\chi_2 = 0.847 \times 10^{-7}$ m ² /s | $\chi = 0.592$ |
| $D_{A1} = 1.1 \times 10^{-9}$ m ² /s | $D_{A2} \approx 1.1 \times 10^{-9}$ m ² /s | $D = 1.0$ |
| $\beta_{T1} = 1.8 \times 10^{-4}$ 1/K | $\beta_{T2} \approx 1.8 \times 10^{-4}$ 1/K | $\beta = 1.0$ |
| $\beta_{A1} = 7.0 \times 10^{-3}$ l/mol | $\beta_{A2} = 12.8 \times 10^{-3}$ l/mol | $\beta_A = 1.83$ |
| $\beta_B = 5.6 \times 10^{-3}$ l/mol | | |
| $\beta_C = 3.5 \times 10^{-3}$ l/mol | | |
| $Q = -5.7 \times 10^4$ J/mol | | |
| $2d = 0.5 \times 10^{-3}$ m | | |
| | $A_0 = 0.25$ mol/l | |

In addition to the set of Eqs. (8)–(21), there is a conservation law for the concentrations. Indeed, as we have supposed that $D_B = D_C$, we can add Eqs. (12) and (13) taking into account the initial and boundary conditions to obtain

$$B(x, z, t) = \frac{1}{\gamma} - C(x, z, t), \quad (22)$$

which is used when the system is studied numerically.

Let us briefly discuss the equations we use. Eqs. (9) and (15) differ from the two-dimensional Navier–Stokes equations by the additional dissipative terms linear in the velocities \vec{v}_1 and \vec{v}_2 . These terms appearing in the Hele–Shaw approximation may be interpreted as the average friction force due to the presence of the plates and are analogous to the linear velocity term in Darcy’s law valid for fluid flow in porous media. The heat Eqs. (10) and (16) contain a cooling term linear in T_1 and T_2 respectively which relates to the dissipation of heat through the solid plates.

In order to model specific experiments, we use the experimental data from Eckert et al. (2004) listed in Table 2. On the basis of these data, we calculate that the Schmidt number is $Sc \approx 980$ while the Lewis number is $Le = 131$. It means that hydrodynamic and heat processes are here quick compared to reaction–diffusion processes. For the set of Rayleigh numbers, we get: $R = 5.34$, $R_A = 2200$, $R_B = 1750$, $R_C = 1100$. By inspecting the density term in Eqs. (9) and (15), this means that heat lowers the density of the solution while the chemical species all contribute to make the solution denser, a solution of A being denser than an equimolar solution of B which is itself denser than that of C . Note that the thermal Rayleigh number is much smaller than the solutal ones which shows that the dynamics in the experiments is here mainly controlled by solutal effects. This is the same as for acid–base reaction fronts in miscible systems where heat effects were also found to be of much smaller amplitude than the solutal ones (Almarcha et al., 2010a, 2011). It is the goal of this article to fix all these values of parameters to focus on changes of dynamics when the Damköhler number D_a and the ratio of initial concentrations γ are varied. Before discussing our results, let us mention that, according to the parameter values in Table 2, one dimensionless unit of time is equal to the characteristic time $\tau = 227$ s while one unit of length is equal to the characteristic length $L_c = 0.5$ mm.

3. Numerical scheme and quantitative measurements

3.1. The solution method

In order to perform two-dimensional simulations of nonlinear regimes, we use the vorticity–stream function formulation of the

governing equations (8)–(21), where the vorticity Φ_i is defined as $\Phi_i = -\Delta\Psi_i$ where Ψ_i is the stream function. A noisy stream function field Ψ_i with amplitude less than 10^{-3} is used in the initial condition.

The described boundary value problem is solved by finite difference methods. The scheme of Simanovskii and Nepomnyashchy (1993), which we have generalized for the reaction–diffusion–convection system in Bratsun and De Wit (2004), was adopted to discretize equations. Equations and boundary conditions are approximated on a uniform mesh using a second order approximation for the spatial coordinates. The non-linear equations are solved using an explicit scheme on a rectangular uniform mesh. The typical resolution was 5×5 nodes for a square of unit side, so that for the domain $H = 40$, $L_{bot} = 40$, $L_{up} = 20$ we use typically 200×300 nodes. In order to ensure the stability of the numerical scheme, the varying time step is calculated at each iteration by the formula

$$\Delta t = \frac{\Delta x^2}{2(2 + \max(|\Psi_i|, |\Phi_i|))}.$$

The Poisson equations are solved by the iterative Liebman successive over-relaxation method at each time step: the accuracy of the solution is fixed to 10^{-4} . The Kuskova and Chudov formulas (Simanovskii and Nepomnyashchy, 1993), providing second order accuracy, are used for the evaluation of the vorticities at the solid boundaries:

$$\Phi_1(x, -L_{bot}) = \frac{1}{2\Delta z^2} (\Psi_1(x, -L_{bot} + 2\Delta z) - 8\Psi_1(x, -L_{bot} + \Delta z)),$$

$$\Phi_2(x, L_{up}) = \frac{1}{2\Delta z^2} (\Psi_2(x, L_{up} - 2\Delta z) - 8\Psi_2(x, L_{up} - \Delta z)).$$

At the interface the expression for the vorticity is approximated with second-order accuracy for spatial coordinates by the formula:

$$\Phi_2(x, 0) = -\frac{2(\Psi_1(x, -\Delta z) + \Psi_2(x, \Delta z))}{\Delta z^2(1 + \eta)}, \quad \Phi_1(x, 0) = \eta\Phi_2(x, 0).$$

Here $\Delta x, \Delta z$ are the mesh sizes for the corresponding coordinates. The temperature and the concentration of A at the interface are calculated by the second-order approximation formula:

$$T_1(x, 0) = T_2(x, 0) = \frac{4T_1(x, -\Delta z) - T_1(x, -2\Delta z) + \kappa(4T_2(x, \Delta z) - T_2(x, 2\Delta z))}{3(1 + \kappa)},$$

$$A_1(x, 0) = A_2(x, 0) = \frac{4A_1(x, -\Delta z) - A_1(x, -2\Delta z) + D(4A_2(x, \Delta z) - A_2(x, 2\Delta z))}{3(1 + D)}.$$

Our code has been successfully tested by comparison with results by Nepomnyashchy and Simanovskii (2001) for two-layer systems with heat release at the interface. In addition, the code recovers known dynamics of the simple reaction–diffusion system. Our results have been tested to be robust with regard to time and space mesh refinements.

3.2. Characterization of the nonlinear dynamics

In order to characterize the nonlinear dynamics resulting from the coupling between chemical reactions and hydrodynamic flows, various types of measurements have been done during the numerical simulations (De Wit, 2004). Let us briefly enumerate them.

At successive times, the two-dimensional concentration fields of $A(x, z, t)$ and $B(x, z, t)$ (or $C(x, z, t)$) can be spatially averaged in the lower layer along either the transverse coordinate x

$$A_x(z, t) = \frac{1}{H} \int_0^H A(x, z, t) dx \quad (23)$$

or the longitudinal coordinate z

$$A_z(x,t) = \frac{1}{L_{bot}} \int_{-L_{bot}}^0 A(x,z,t) dz, \quad (24)$$

to yield one-dimensional averaged profiles $A_x(z,t)$ and $A_z(x,t)$ respectively. The transversed averaged profile (23) gives insight into the

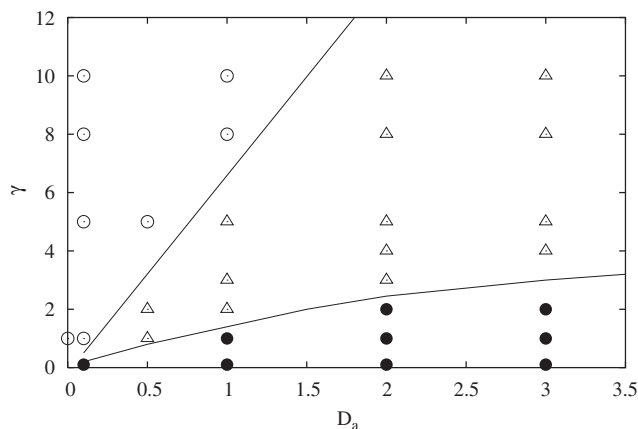


Fig. 2. Classification of the various dynamic regimes in the parameter plane spanned by the ratio of initial reactant concentrations γ versus the Damköhler number D_a . The lines delimit approximately the regimes dominated by hydrodynamics (\circ), chemistry (\bullet) or by a mixture of these (\triangle).

speed and intensity of invasion of the lower layer by the reaction front and by convective currents. The longitudinal averaged profile (24) allows on the other hand to follow the interaction between fingers.

The transverse averaged profile (23) is next used to define the tip and rear of the fingered zone. The tip is chosen arbitrarily as the location along the z -axis in front of which the averaged concentration $A_x(z,t)$ is less than 0.001. The position of the rear is nothing else than the location of the interface $z=0$. Thus, the position of the tip defines automatically the mixing length (which is the distance between the tip and the rear of the fingered zone).

If the chemical reactions affect the hydrodynamic fingering, fingering also has an influence on the reaction rate. Indeed in a fingered front, it is expected that the rate of reaction will speed up because of the convective movements of the fluid. In that respect, an interesting measure is given by the reaction rate R computed in terms of the area of the reacted zone (i.e. the number of points where $C(x,z,t)$ is larger than an arbitrary threshold C^*) normalized by the width of the system versus time. In other words, we compute as a function of time the quantity

$$R(t) = \frac{1}{HL_{bot}} \int_{-L_{bot}}^0 \int_0^H \zeta dx dz, \quad (25)$$

where $\zeta = 1$ if $C(x,z,t) > C^*$ (C^* is typically 0.001 here) and zero otherwise.

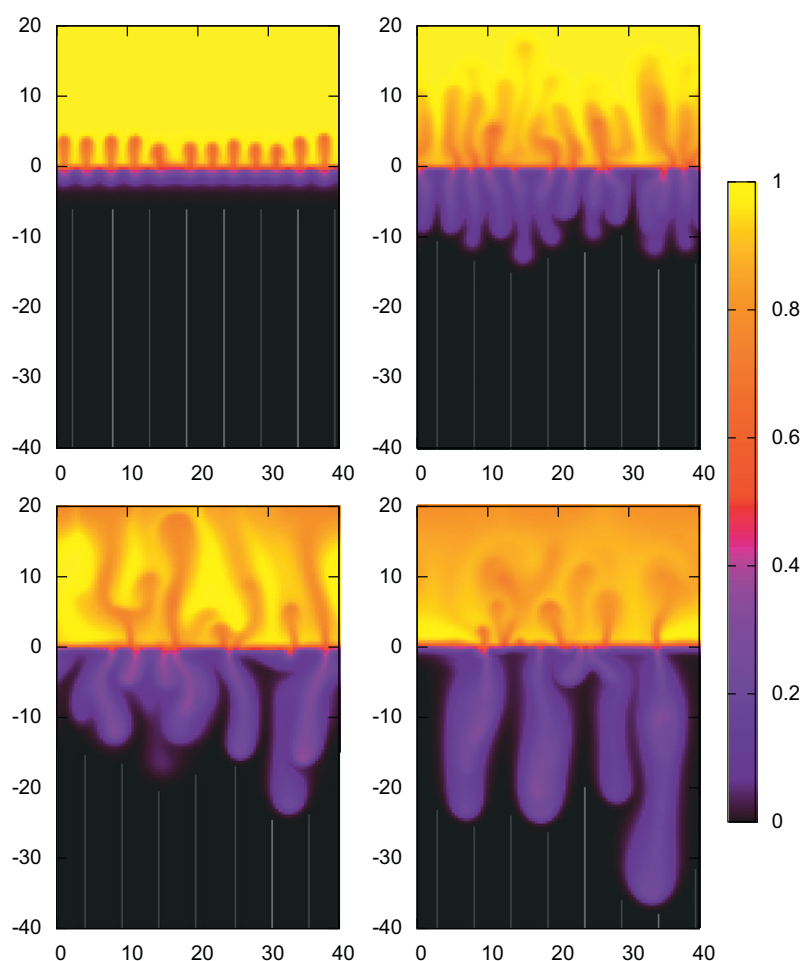


Fig. 3. Density plots of the concentration of species A showing the dynamics in the absence of reaction: $D_a=0$, $\gamma=1$. The frames from left to right and from up to down correspond to times $t=1.2, 2.2, 3.2, 4.0$ respectively. The domain of integration is $0 < x < 40$, $-40 < z < 20$.

The mass transfer rate M of A through the interface and its dependence on reaction and convection is of special interest from different points of view. A convenient quantitative characteristic of this process can be defined as

$$M(t) = \frac{\int_0^H \frac{\partial A_1(x,z,t)}{\partial z} \Big|_{z=0} dx}{\int_0^H \frac{\partial A_1^{\text{diff}}(x,z,t)}{\partial z} \Big|_{z=0} dx}, \quad (26)$$

where $A_1^{\text{diff}}(x,z,t)$ is the concentration of A in the pure reaction–diffusion regime. This definition is similar to that of the Nusselt number formulated for heat. Eventually, a convenient quantitative measure of the dynamic change of the wavelength of the pattern is provided by the power averaged mean wavenumber defined as

$$k(t) = \frac{\sum k_i P_i}{\sum P_i}, \quad (27)$$

where k_i are the Fourier modes of the Fourier transform of the longitudinal averaged profile (24) and P_i their amplitude in Fourier space.

4. Nonlinear simulations

4.1. Overview

As described in Eckert and Grahn (1999) and Eckert et al. (2004), the origin of convection in the upper layer is a diffusive

layer convection (DLC) mechanism (Trevelyan et al., 2011) whereby the acid rich zone on top of the cell overlies the acid depleted region just above the interface. This depletion is the result of the transfer of the acid towards the lower layer. This mechanism is similar to the one occurring for fast downward diffusing acids responsible for the plumes observed above the initial contact line in miscible systems (Almarcha et al., 2010a, 2011).

In the lower layer of the immiscible stratification, convection originates from a Rayleigh–Taylor instability induced by the diffusion into the lower layer of the reactant A . In the absence of reaction, this leads in the lower aqueous phase to a boundary layer of A on top of a less dense bulk solution of B because $R_A > R_B$ which triggers convection into fingers slowly invading the lower layer. This explains the experimental observation of convection in the same system with pure diffusion of A without reaction (Eckert and Grahn, 1999; Eckert et al., 2004), a situation for which the effect of the reaction product C and of heat can be ignored. Numerical simulation of our equations indeed demonstrate appearance of convection even in this simplified case which shows that the basic instability in the lower layer is not related to double-diffusion (excluded here as $D_A = D_B$) (Trevelyan et al., 2011; Almarcha et al., 2010a) but to a Rayleigh–Taylor mechanism. This might not be true for other values of the Rayleigh numbers, but for the above fixed values calculated from experimental data, only density fingering was found. Let us note that no fingering occurs below the contact line for miscible experiments done with HCl/NaOH (Almarcha et al., 2010a, 2011) because in

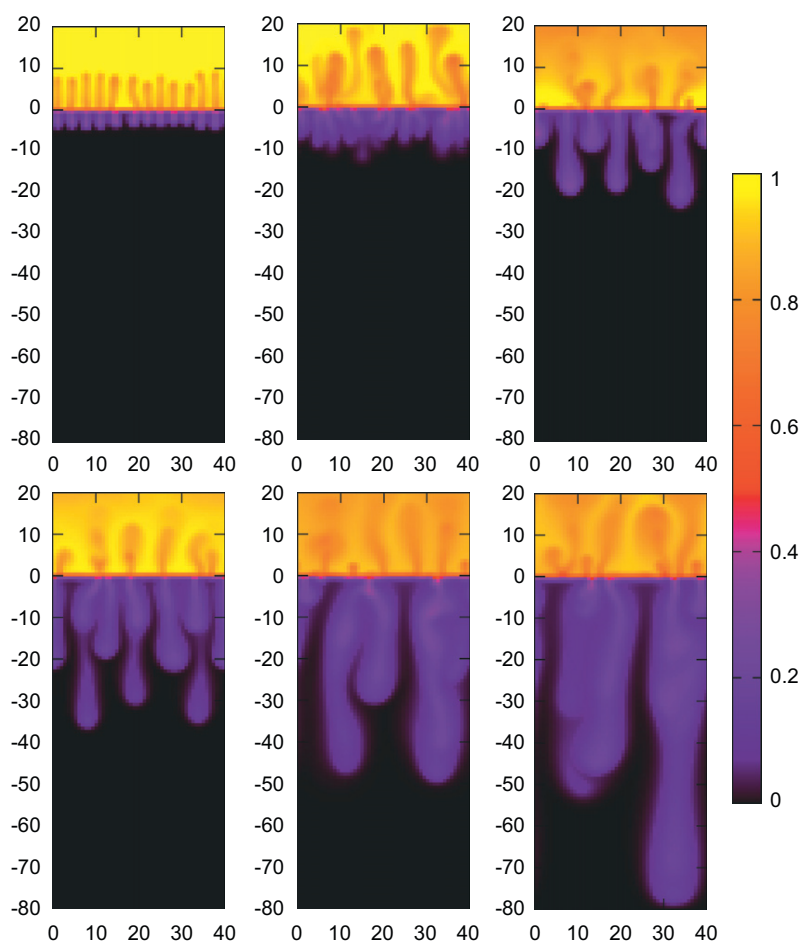


Fig. 4. Density plots of the concentration of species A showing the dynamics in the presence of a chemical reaction: $D_a = 3$ and $\gamma = 10$. The frames from left to right and from up to down correspond to times $t = 1.4, 2.6, 3.8, 5.0, 11.0, 15.0$ respectively. The domain of integration is $0 < x < 40, -80 < z < 20$.

this special case the acid is less dense than the base but most importantly it is consumed by the reaction and is replaced by a less dense salt diffusing upwards which avoids the accumulation of a locally denser boundary layer responsible for downward fingering in the immiscible case.

Let us now focus on the immiscible case and analyze to what extent the chemical reaction changes the characteristics of the instability and impacts pattern formation. Fig. 2 classifies the dynamics in the parameter plane γ versus D_a , where three different types of pattern formation were found. Open circles indicate a “pure” density fingering similar to the one observed in the absence of reaction, triangles denote fingering extending far into the lower layer with a strong reaction effect while black circles correspond to a regime of small extent fingering confined near the interface. The lines draw approximate limits between these three cases. Figs. 3–6 show how the pattern evolves in each characteristic case. Let us consider them in detail.

4.2. “Pure” density fingering

When chemistry is playing a minor role as for the open circles in Fig. 2, the dynamics is similar to the one obtained in the absence of any reaction, i.e. for $D_a=0$, $\gamma=1$ as shown in Fig. 3. The open circles on Figs. 7–9 present for these values of parameters the $A_x(z,t)$ profile at $t=4$ (Fig. 7a), the location $Z(t)$ of the finger tip (Fig. 7b), the $A_z(x,t)$ profile at $t=4$ (Fig. 8a), the power averaged

wavenumber $k(t)$ (Fig. 8b), the time evolution of the stream function maximum (Fig. 9a) and the mass transfer rate $M(t)$ (Fig. 9b). The dynamics of the system can be divided in four stages. First, a diffusive process (or a reaction–diffusion one if $D_a \neq 0$) takes place (see Fig. 7b). Then, convection arises, first in the upper layer where the depletion of A close to the interface leads to an unstable density stratification (DLC mechanism Trevelyan et al., 2011) similar to the one seen in miscible systems (Almarcha et al., 2010a, 2011). Due to the interaction through the interface, convection above helps to develop flows in the lower layer. On the other hand, A diffusing into the lower layer produces a denser sublayer located just below the interface providing locally a stratification which is unstable with respect to Rayleigh–Taylor disturbances. The resulting convection in the lower layer leads to the onset of the fingering process (Fig. 3), to a sharp increase of the amplitude of the stream function (Fig. 9a) and of the reactant mass transfer through the interface (Fig. 9b). It manifests itself also in the acceleration of the movement of the finger tip far away from the interface shown in Fig. 7b. The average wavenumber of fingers at this stage is about $k \approx 2$ (the wavelength is about 3 units of length or 1.5 mm). As time goes by, the vortices and consequently the fingers become wider, i.e. the wavenumber permanently decreases with time (Fig. 8b). This tendency can be explained by a weakening of the unstable gradient of A in the course of time.

At about $t \approx 2.2$ the dynamics changes again: the wavenumber of the pattern has become such that the fingers do not enlarge any

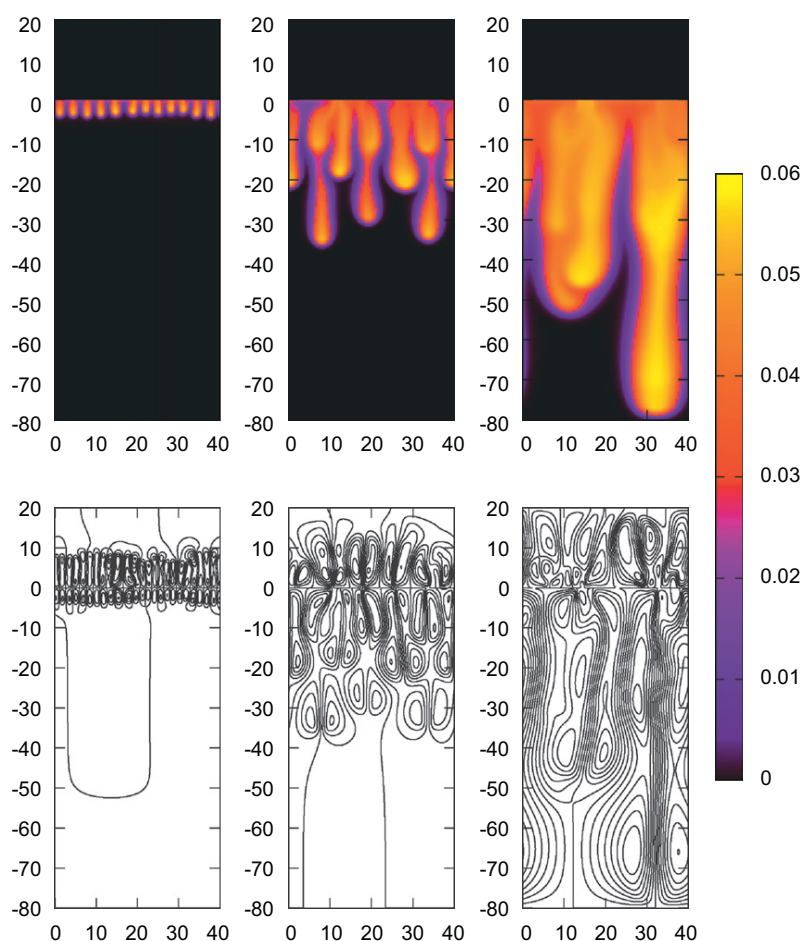


Fig. 5. Evolution of the concentration of C (top) and of the stream function (bottom) in the reactive case of Fig. 4. The stream function varies in the range: $-20 < \Psi_1 < 20$, $-30 < \Psi_2 < 30$ (left); $-35 < \Psi_1 < 35$, $-25 < \Psi_2 < 25$ (center); $-50 < \Psi_1 < 50$, $-20 < \Psi_2 < 20$ (right). $t=1.4, 5.0, 15.0$ from left to right.

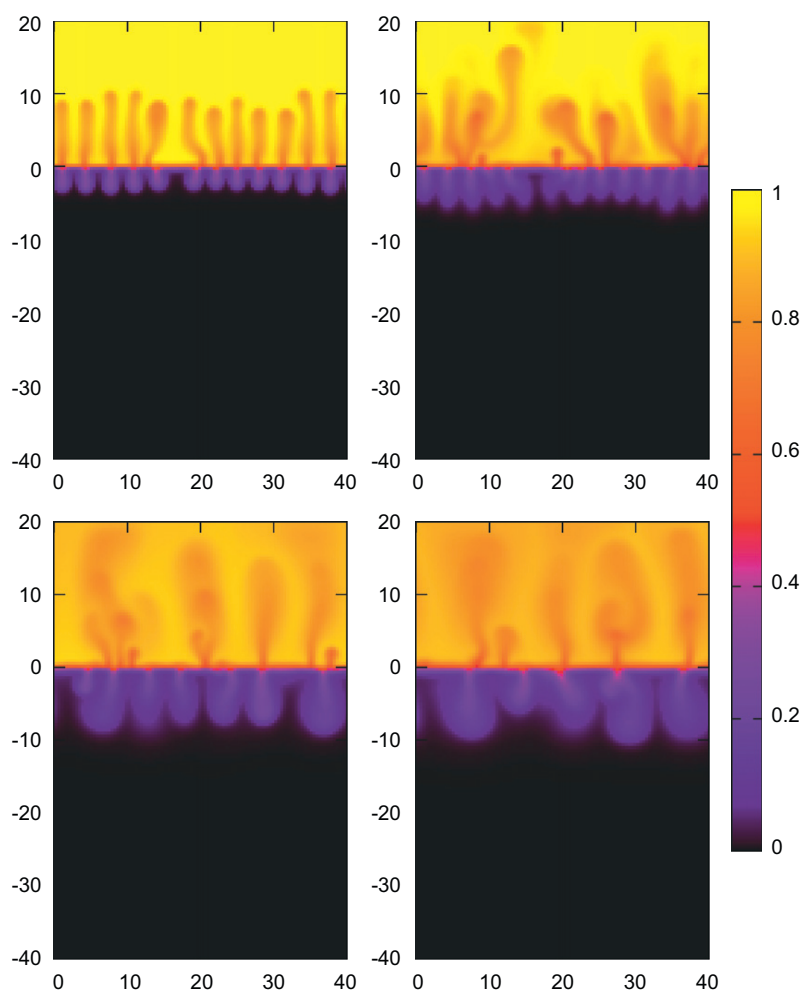


Fig. 6. Density plots of A for $D_a=1$, $\gamma=1$. The frames from left to right and from up to down pertain to times $t=1.4, 2.2, 6.0, 10.0$ respectively. The domain of integration is $0 < x < 40$, $-40 < z < 20$.

more by just widening along the interface and, as a consequence, they do not penetrate deeper in the lower layer. The system enters in a regime which could be called “predominantly diffusive” characterized by a square root type of growth for the tip movement (Fig. 7b). The dominance of diffusion can also be seen in Fig. 3 (second frame above), where the boundaries between fingers appear smoother in comparison with previous or following stages. After the wavenumber of the pattern has decreased sharply to 0.5 at about $t \approx 3$, the stream function increases and hydrodynamics dominates again over diffusion. A quick propagation of fingers (now with larger wavelength) is then observed deeply inside the lower layer (Fig. 7b). It is interesting to note that the “motor” of fingering is here a pair of intensive vortices extending downwards from the interface and penetrating deeper and deeper inside the lower layer. The fluid flow inside the vortices circulates such as to pull fresh A downward (Fig. 3, lower row) in the middle of the fingers as observed experimentally (Eckert et al., 2004). This general spatiotemporal dynamics is observed for all points denoted by open circles in Fig. 2. When γ is increased, this pattern is observed for an increased set of D_a . This is due to an increasing influence of denser A for a given small value of C as the initial concentration A_0 is increased for a fixed value of B_0 . In the presence of chemical reactions ($D_a \neq 0$), the heat effect produced by the reaction just below the interface reinforces the plumes in the upper layer by a Rayleigh–Bénard mechanism.

4.3. Reactive fingering

Let us now consider non-linear dynamics and pattern formation for a stronger effect of reaction: $D_a=3$, $\gamma=10$. This case characterizes generally the processes happening in the domain indicated in Fig. 2 by open triangles. The equations were integrated in a longer domain $-80 < z < 20$ in order to trace the dynamics up to later times. Fig. 4 shows the temporal evolution of the concentration of A while Fig. 5 shows the dynamics of the C concentration (upper row) and of the stream function (lower row) respectively. The quantitative properties of the dynamics are shown for these values of parameters by open triangles in Figs. 7–9.

The system evolves through four stages as in the previous case: reaction–diffusion ($0 < t < 1.4$), onset of fingering ($1.4 < t < 2.0$), dominance of diffusion over convection ($2.0 < t < 3.0$) followed by fingering again after the wavenumber of pattern decreases ($t > 3.0$). All these stages lead to a sharp change in the fingers propagation speed (Fig. 7b) and in the mass transfer rate (Fig. 9b). But in this case where chemical reactions are quite efficient, the action of the Rayleigh–Taylor instability is more complicated than in the previous case. Now three species are interplaying in the density profile. By inspecting the experimental data listed in Table 2, we see that the solutal expansion coefficient is maximal for A , slightly less for B and minimal for C ($R_A > R_B > R_C$). It means that we still have a buoyantly unstable density stratification as the density gradient is positive

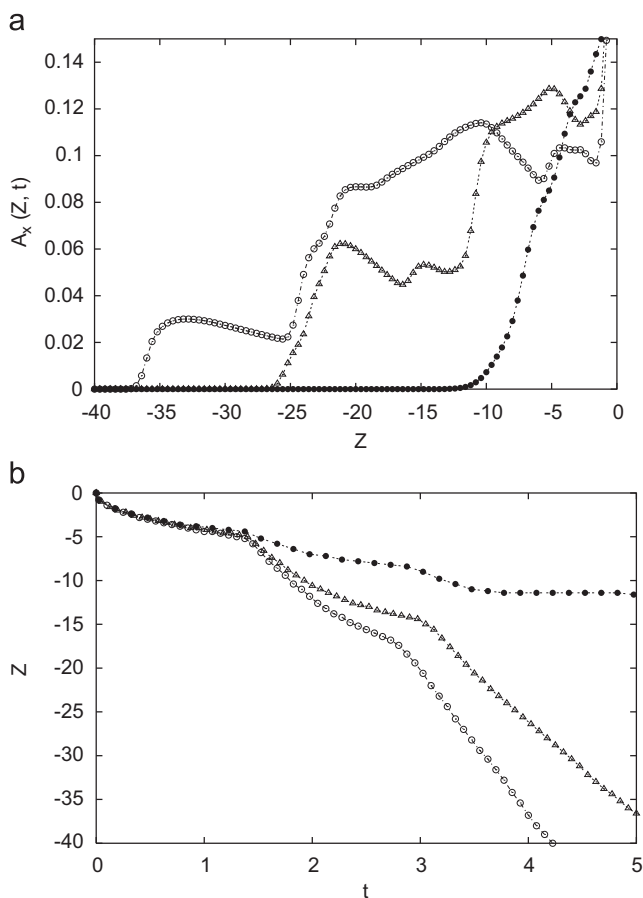


Fig. 7. (a) Transverse averaged profile of concentration $A_x(z,t)$ at time $t=4.0$ and (b) time evolution of finger tip shown for the three main types of pattern formation. Open circles: $D_a=0$, $\gamma=1$ as in Fig. 3; open triangles: $D_a=3$ and $\gamma=10$ as in Figs. 4 and 5; dark circles: $D_a=1$, $\gamma=1$ as in Fig. 6.

when going from the concentrated B solution to the upper A one. But when the reaction starts, lighter C , which is produced in the reaction zone between A and B , replaces both reactants and, being less dense than them, stabilizes locally the system. Thus, one can *a priori* expect that the Rayleigh–Taylor instability will be less intense and will then induce a more complicated pattern.

This is indeed the case. The most striking difference with the case of hydrodynamic density fingering of Fig. 3 is the appearance of a quite regular pattern at about $t \approx 3$ (Figs. 4 and 5). The stream function features now a vertical chain of counter-rotating short vortices instead of the sole long vortex observed in the previous regime (see Fig. 5, second column). This chess-like structure persists in time despite the fact that the wavenumber of the pattern grows in time (Fig. 5, last column).

In order to observe such a pattern experimentally, one can increase the initial concentration A_0 and B_0 keeping their ratio γ constant but changing in this way the Damköhler number $-(2d)^2 k_c A_0 / D_{A1}$ – moving thus to the right in the (D_a, γ) parameter plane. It is however necessary to realize that the Rayleigh numbers will then also vary complicating the situation.

4.4. Interfacial convection: mild fingering

Eventually, let us consider the case where only mild fingering is observed (lower part in Fig. 1 indicated by black circles). As an example, consider the case for which $D_a=1$, $\gamma=1$. Fig. 6 shows the time evolution of the concentration of A while the various

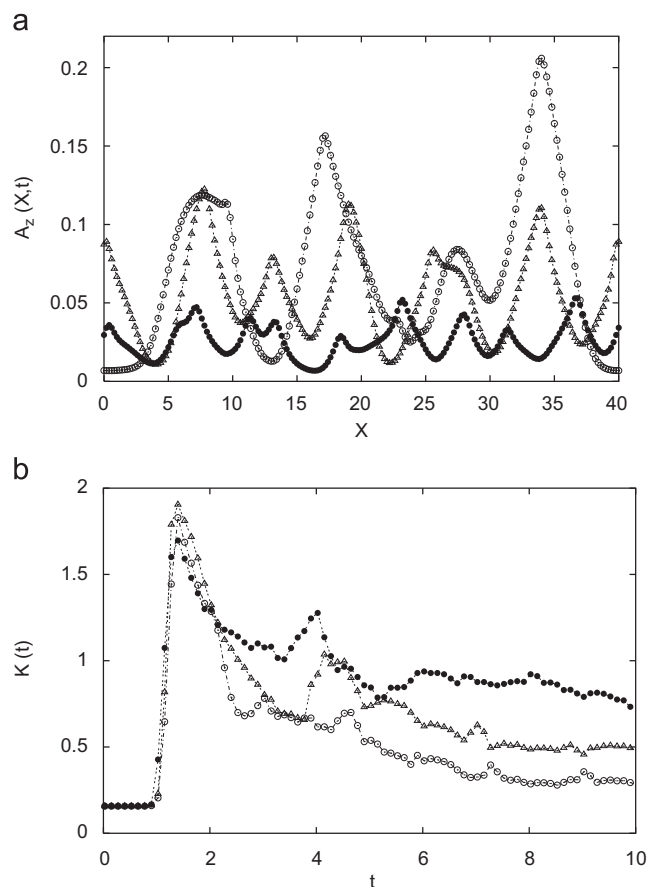


Fig. 8. Longitudinally averaged profile of $A_z(x,t)$ at time $t=4.0$ (a) and (b) time evolution of the power averaged mean wavenumber k shown for the three main types of pattern formation. Symbols and values of parameters as in Fig. 7.

quantitative measures quantifying the dynamics for these values of parameters are shown in Figs. 7–9 by black circles.

As can be seen from these figures, this dynamics is characterized in the lower layer by a weak invasion of A (Fig. 7b), a low intensity of hydrodynamic flow (Fig. 9a) and a smaller mass transfer through the interface (Fig. 9b). In fact, the fluid dynamics remains localized near the interface and no developed fingering is observed below the interface. This can be explained as follows: if the Damköhler number increases, the chemical time scale is decreasing, the reaction prevails over the hydrodynamics and consequently a larger amount of product C is produced per unit of time. A zone of C solution which is substantially less dense and hotter than those of the overlying A and underlying B prevents the fingers from invading the lower part of the system. The upper unstable transition zone between A and C is then subdued by a stable transition zone between C and B . The Rayleigh–Taylor instability in this case remains confined into a boundary layer close to the interface because of the high rate of A consumption during the reaction.

It should be noted that between the mild fingering domain and the domain of predominantly reactive fingering in the parameter plane of Fig. 1 there is a transition region with intermediate regimes. A solid line delimiting the two zones is drawn as a guide to the eye and is thus not a bifurcation curve. A smooth transition is actually observed in between these domains.

4.5. Parametric study

Let us now consider the particular effect on the fingering dynamics of the ratio of initial concentrations $\gamma = A_0/B_0$ (Fig. 10)

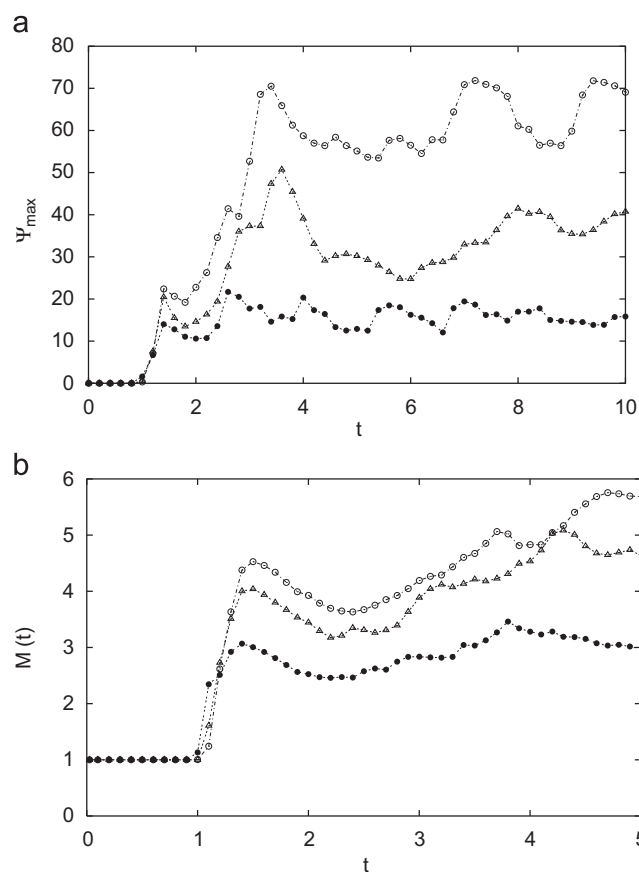


Fig. 9. Temporal evolution of (a) the stream function's maximum Ψ_{\max} and (b) of the mass transfer rate M . Symbols and values of parameters as in Fig. 7.

and of the Damköhler number D_a (Fig. 11). To do so we follow the temporal evolution of the reaction rate R and of the position of the tip of the fingers. Fig. 10 shows that, for a fixed value of D_a , the system is more unstable when γ is increased. This increase leads indeed to much more intense fingering witnessed by a strong increase in $R(t)$ (Fig. 10a) and in the increase of the invasion length of the fingers in the lower layer (Fig. 10b). When $\gamma = 0.1$, B is largely in excess compared to A . Any molecule of A diffusing across the interface will quickly be converted into the product C leading to a stable stratification of less dense C above denser B . No visible fingering takes place in that case and the reaction rate grows diffusively in time while the position of the reaction front remains pinned close to the interface. When $\gamma = 1$, i.e. in a situation of equimolar initial concentration of A and B , fingers slowly invade the lower layer and organize themselves quite regularly as seen on Fig. 4 and also observed in experiments (Eckert et al., 2004). The strongest fingering occurs for $\gamma > 1$ when A is in excess (Eckert et al., 2004). In that case, the reaction front invades the lower layer and the excess of denser A on top of the less dense product C and reactant B makes the system strongly Rayleigh–Taylor unstable.

If now, the ratio of initial concentrations γ is fixed to a constant value but the Damköhler number D_a is varied (see Fig. 11), we observe that the most unstable situation is the non-reactive case $D_a \rightarrow 0$. Indeed, for the values of parameters related to the experiments conducted by Eckert and Grahn (1999) and Eckert et al. (2004), $R_A > R_B > R_C$ and the solution of species A is the denser one. Hence, the larger the amount of A crossing the interface and invading the lower layer, the more unstable the density stratification of dense A on top of less dense B . When D_a is increased, the chemical

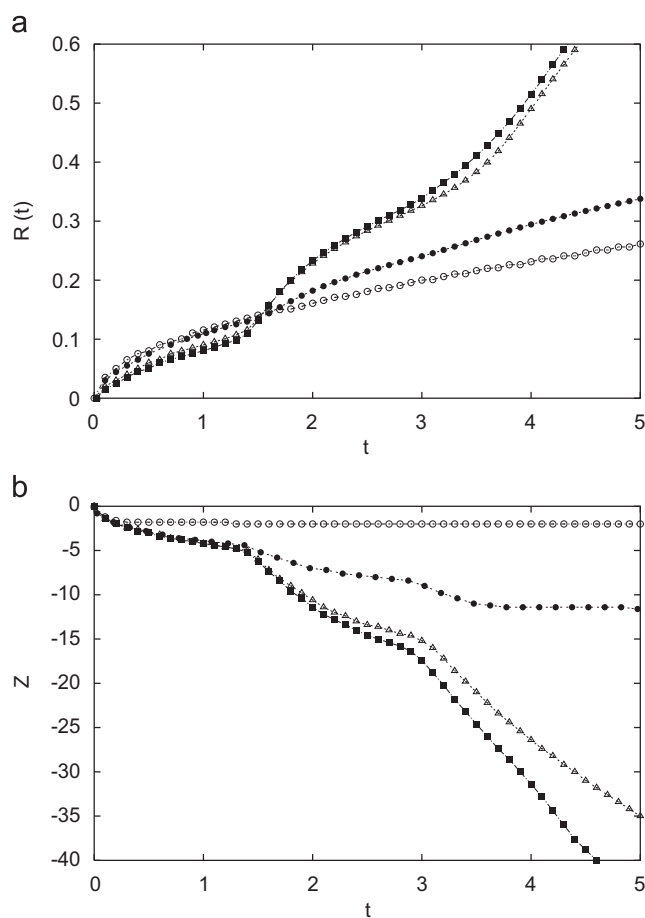


Fig. 10. Temporal evolution of (a) the reaction rate R and (b) of the fingers tip position shown for four different values of the initial concentration ratio $\gamma = 0.1$ (\circ); 1 (\bullet); 5 (\triangle); 10 (\blacksquare) for a fixed Damköhler number $D_a = 1$.

reaction becomes more effective and more A is converted into C per unit time. This replaces A by less dense C which is stabilizing the system as seen in Fig. 11 which shows a decrease in R and in the invasion by fingers of the lower layer when D_a is increased. For infinitely large D_a , A is instantaneously converted into C which drives a stable stratification of C above denser B . The growth of the reaction rate and the position of the reaction front evolve then diffusively in time as shown in Fig. 11 for $D_a = 3$.

4.6. Comparison with experiments

To make more quantitative comparison with experiments, we note that in the experiments by Eckert et al. (see Fig. 2c of Eckert et al., 2004), the wavelength λ of the regular fingers seen in the lower layer is of the order of 3.5 mm at a dimensional time $t_d = 22$ min (1320 s) for $\gamma = 1$. Recalling that, in our non-dimensionalization scheme, our characteristic length $L_c = 0.5$ mm and time $\tau = 227$ s, this corresponds to a dimensionless wavenumber $k = 2\pi L_c / \lambda = 0.9$ at a dimensionless time $t = t_d / \tau = 5.8$, which is in excellent agreement with the value of $k(t)$ given in Fig. 8b for $\gamma = 1$ (black circles). Moreover, Fig. 4 of Eckert et al. (2004) confirms our observation that the length of the fingers is larger when γ is increased at fixed Da (as shown when comparing with our Fig. 10).

Comparison with experiments has however also some difficulties as we do not exactly know the value of the Damköhler number as we do not have the value of the kinetic constant k_c . Besides, our simulations are done here with equal diffusion coefficients for all

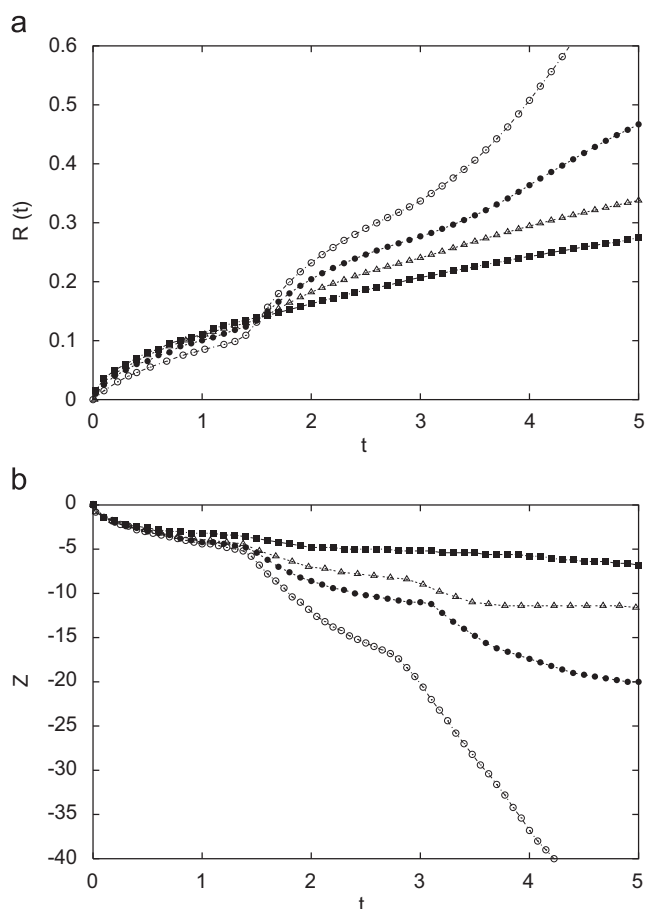


Fig. 11. Temporal evolution of (a) the reaction rate R and (b) of the finger tip position shown for four different values of the Damköhler number $Da=0.1$ (\circ), 0.5 (\bullet), 1 (\triangle), 3 (\blacksquare) for a fixed initial concentration ratio $\gamma=1$.

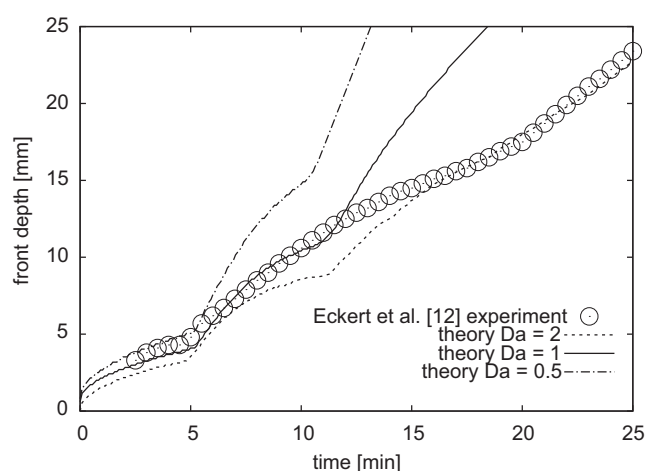


Fig. 12. Comparison in dimensional units between experimental (from Fig. 5 of Eckert et al., 2004) and numerical position of the tip of the fingers in the lower layer for $\gamma=4$ and $Da=0.5, 1$ and 2 .

species which kills any possible solutal double diffusive instabilities (Trevelyan et al., 2011). The resulting difficulty is best illustrated in Fig. 12 where we compare the position of the tip of the fingers in the lower layer obtained experimentally (see Fig. 5 of Eckert et al., 2004) with those converted in dimensional units for $\gamma=4$ and three different values of Da . While the agreement is quantitative in the

early stages, discrepancies increase later on depending on the value of Da when fingers are in well developed nonlinear regimes. As these nonlinear dynamics are also particularly sensitive to initial conditions and on noise (see De Wit et al., 2005, for a discussion on the sensitivity of nonlinear dynamics to the noise seeding initial conditions), this highlights the interest but also limitations of comparison with experiments.

5. Discussion and conclusions

In immiscible two-layer systems oriented vertically in the gravity field, convection can set in upon diffusion of a chemical species A from the upper to the lower layer where a species B is initially dissolved. We have here analyzed numerically the influence of an exothermic chemical reaction $A+B\rightarrow C$ taking place solely in the lower layer on such a buoyancy-driven instability of Rayleigh–Taylor type. To do so, we have numerically integrated a reaction–diffusion–convection model coupling the evolution of concentrations and temperature to the flow field inside a 2D Hele–Shaw cell. Fixing the Rayleigh numbers of the problem to values computed for experimental data available in the literature (Eckert and Grahn, 1999; Eckert et al., 2004), we study the changes in dynamics as a function of the Damköhler number Da of the problem and of the ratio of initial reactant concentrations γ . Depending whether A initially dissolved in the upper layer is in excess or not, the Rayleigh–Taylor fingers developing in the lower layer will be very elongated or only limited to a small boundary layer close to the interface. If A is in excess, it will develop after diffusion into the lower layer a zone of denser solution of A on top of less dense solutions of product C and bulk reactant B . This favors the growth of long and elongated density fingers in the lower layer. On the contrary, when the reactant B present in the lower layer is in excess, the reaction zone remains confined close to the interface and convection remains of small finite amplitude. The most regular fingers are obtained for intermediate situations when the initial concentrations of A and B are of the same order of magnitude. To quantify the dynamics we have computed various properties of the system like typically the reaction rate and the speed of reaction front as a function of time. We find that both quantities increase with γ but decrease with Da .

The present work has fixed the Rayleigh values of the problem to those computed for the experiments performed by Eckert and Grahn (1999) and Eckert et al. (2004). It will be of interest in the future to analyze to what extent the dynamics depend in particular on these parameters. Indeed, changing the nature of chemical species at fixed initial concentrations has been shown to have a drastic influence on the fingering pattern (Eckert and Grahn, 1999).

Acknowledgments

We wish to thank K. Eckert, V. Pimienta, M. Acker and Y. Shi for stimulating discussions and for sharing their experimental results with us prior to publication. This work has been financially supported by Prodex, ESA and FNRS. D.B. wishes to thank the Office for Scientific, Technical and Cultural Affairs (Belgium) and Administration of Perm Region, Russia (RFBR 07-01-96043) for their financial support.

References

- Almarcha, C., Trevelyan, P.M.J., Grosfils, P., De Wit, A., 2010a. Phys. Rev. Lett. 104, 044501.
- Almarcha, C., Trevelyan, P.M.J., Riolfo, L., Zalts, A., El Hasi, C., D'Onofrio, A., De Wit, A., 2010b. J. Phys. Chem. Lett. 1, 752–757.

- Almarcha, C., R'Honi, Y., De Decker, Y., Trevelyan, P.M.J., Eckert, K., De Wit, A., 2011. *J. Phys. Chem. B* 115, 9739–9744.
- Avnir, D., Kagan, M.L., 1984. Spatial structures generated by chemical reactions at interfaces. *Nature* 307, 717–720.
- Avnir, D., Kagan, M.L., 1995. The evolution of chemical patterns in reactive liquids, driven by hydrodynamic instabilities. *Chaos* 5, 589–601.
- Bees, M.A., Pons, A.J., Sorensen, P.G., Sagues, F., 2001. Chemoconvection: a chemically driven hydrodynamic instability. *J. Chem. Phys.* 114, 1932–1943.
- Bratsun, D.A., De Wit, A., 2004. On Marangoni convective patterns driven by an exothermic chemical reaction in two-layer systems. *Phys. Fluids* 16, 1082–1096.
- Bratsun, D.A., Shi, Y., Eckert, K., De Wit, A., 2005. Control of chemo-hydrodynamic pattern formation by external localized cooling. *Europhys. Lett.* 69, 746–752.
- Citri, O., Kagan, M.L., Kosloff, R., Avnir, D., 1990. Evolution of chemically induced unstable density gradients near horizontal reactive interfaces. *Langmuir* 6, 559–564.
- De Wit, A., 2004. Miscible density fingering of chemical fronts in porous media: nonlinear simulations. *Phys. Fluids* 16, 163–175.
- De Wit, A., Bertho, Y., Martin, M., 2005. Viscous fingering of miscible slices. *Phys. Fluids* 17, 054114.
- Eckert, K., Grahn, A., 1999. Plume and finger regimes driven by a exothermic interfacial reaction. *Phys. Rev. Lett.* 82, 4436–4439.
- Eckert, K., Acker, M., Shi, Y., 2004. Chemical pattern formation driven by a neutralization reaction. I: mechanism and basic features. *Phys. Fluids* 16, 385–399.
- Ermakov, S.A., Ermakov, A.A., Chupakhin, O.N., Vaisov, D.V., 2001. Mass transfer with chemical reaction in conditions of spontaneous interfacial convection in processes of liquid extraction. *Chem. Eng. J.* 84, 321–324.
- Grahn, A., 2006. Two-dimensional numerical simulations of Marangoni-Bénard instabilities during liquid-liquid mass transfer in a vertical gap. *Chem. Eng. Sci.* 61, 3586–3592.
- Karlov, S.P., Kazenin, D.A., Vyazmin, A.V., 2002. The time-evolution of chemo-gravitational convection on a brim meniscus of wetting. *Physica A* 315, 236–242.
- Micheau, J.-C., Gimenez, M., Borckmans, P., Dewel, G., 1983. Hydrodynamic instabilities and photochemical reactions. *Nature* 305, 43–45.
- Nepomnyashchy, A.A., Simanovskii, I.B., 2001. Nonlinear investigation of anti-convection and Rayleigh-Bénard convection in systems with heat release at the interface. *Eur. J. Mech. B/Fluids* 20, 75.
- Pérez-Villar, V., Muñuzuri, A.P., Pérez-Muñuzuri, V., 2000. Convective structures in a two-layer gel-liquid excitable medium. *Phys. Rev. E* 61, 3771–3776.
- Pons, A.J., Sagues, F., Bees, M.A., Sorensen, P.G., 2000. Pattern formation in the Methylene-Blue-Glucose system. *J. Phys. Chem. B* 104, 2251–2259.
- Sherwood, T.K., Wei, J.C., 1957. Interfacial phenomena in liquid extraction. *Ind. Eng. Chem.* 49, 1030–1034.
- Shi, Y., Eckert, K., 2006. Acceleration of reaction fronts by hydrodynamic instabilities in immiscible systems. *Chem. Eng. Sci.* 61, 5523–5533.
- Shi, Y., Eckert, K., 2007. Orientation-dependent hydrodynamic instabilities from chemo-Marangoni cells to large scale interfacial deformations. *Chin. J. Chem. Eng.* 15, 748–753.
- Shi, Y., Eckert, K., Acker, M., Heinze, A., 2005. The chemically driven interfacial convection (CDIC) experiment on MASER 10. In: *Proceedings of the 17th ESA Symposium on European Rocket and Balloon Programmes and Related Research*, Sandefjord, Norway (ESA SP-590).
- Simanovskii, I.B., Nepomnyashchy, A.A., 1993. *Convective Instabilities in Systems with Interface*. Gordon and Breach, London.
- Trevelyan, P.M.J., Almarcha, C., De Wit, A., 2011. *J. Fluid Mech.* 670, 38–65.
- Zalts, A., El Hasi, C., Rubio, D., Ureña, A., D'Onofrio, A., 2008. *Phys. Rev. E* 77, 015304R.